Green Chemistry

PAPER

View Article Online
View Journal | View Issue

Check for updates

Cite this: *Green Chem.*, 2024, **26**, 8794

Novel diacid–superbase ionic liquids for efficient dissolution of cellulose and simultaneous preparation of multifunctional cellulose materials†

Long Zhang, Boxiang Zhan, Yapeng He, Yongqi Deng, Haiyuan Ji, Shen Peng and Lifeng Yan *

Green and sustainable cellulose-based materials are of increasing interest to researchers due to the energy crisis and environmental pollution. However, developing green solvents for cellulose is still a big challenge. No longer limited to monoacid-superbase ionic liquids (ILs), this work innovatively proposes novel diacid–superbase ionic liquids that maximally dissolve 15.2 wt% of microcrystalline cellulose (DP = 260) and 9.3 wt% of cotton wool (DP = 685), respectively. The effects of the structure of ILs on cellulose solubility and the interactions between ILs and cellulose during dissolution were analyzed by comparing different types of diacids and superbases. For sustainability, the ILs can be recycled and reused to dissolve cellulose. In addition, the rheological properties of the cellulose solutions were studied for fiber spinning. The cellulose solutions had strong attractive interactions with the substrates and showed universal bonding properties, achieving tensile strengths of 2.39 MPa and 2.28 MPa for wood and bamboo boards, respectively. Through regeneration in a solidification bath and hot pressing, the regenerated cellulose films show structural integrity, dense morphology, a high degree of crystallinity, excellent tensile strength (134 MPa), sufficient thermal stability, and excellent transparency. Finally, the prepared cellulose gel was incorporated into a zinc-ion hybrid supercapacitor (ZHSC) with a wide voltage window, high energy and power density, and excellent cycling performance. In summary, this work presents diacid–superbase ionic liquids for the efficient dissolution of cellulose for the first time. Meanwhile, a variety of high-performance cellulosic materials were prepared, which greatly enrich the possibilities for the use of ILs in the production of functional cellulosic materials.

Received 28th April 2024,
Accepted 24th June 2024

DOI: 10.1039/d4gc02083a

rsc.li/greenchem

Published on 27 2024. Downloaded on 14/05/2026 05:56:35.

Introduction

The continuous growth of the world's population and rapid economic development in recent years have led to the overconsumption of non-renewable resources (coal, oil, natural gas, *etc.*), which has led to a series of natural disasters, including large-scale pollution of the natural environment and extreme climate changes.[1,2] Reducing dependence on non-renewable resources and developing renewable resources have attracted a great deal of attention.[3–5]

Cellulose is the most abundant biopolymer on Earth, and it is found mainly in plants as a structural component of cell walls.[6] Plants all over the world produce more than ten billion tonnes of cellulose each year, making cellulose the largest reservoir of organic carbon.[7,8] Cellulose is a linear polymer composed of dehydrated glucosyl units linked by β (1 → 4) glycosidic bonds.[6,9] As a natural polymer, cellulose is widely used in textiles, packaging, construction, medicine, and biochemistry because of its low cost, ease of modification, high mechanical strength, renewability, biocompatibility, and biodegradability.[10–14] However, there exist hydrogen bonding network structures in cellulose, where three hydrogen bonding structures are formed around each glucosyl unit: an intermolecular hydrogen bond and two intramolecular hydrogen bonds.[15] These large and complex hydrogen bonding network structures of cellulose result in a high degree of crystallinity and stability, making cellulose insoluble in water and most conventional organic solvents.[16,17]

Cellulose dissolution is a crucial step in the processing of cellulosic materials. Therefore, researchers have continued to develop solvent systems to dissolve cellulose, including *N*-methyl morpholine-*N*-oxide (NMMO),[18,19] LiCl/N, *N*-dimethylacetamide (LiCl/DMAc),[20,21] NaOH solutions,[22–25] tetrabutylammonium fluoride/dimethyl sulfoxide systems,[26,27] metal complex solutions,[28] molten inorganic salt hydrates,[29,30] ionic liquids (ILs),[31] and deep eutectic solvents (DESs).[32,33]

Key Laboratory of Precision and Intelligent Chemistry, and Department of Chemical Physics, University of Science and Technology of China, Jinzhai Road 96, Hefei, 230026 Anhui, China. E-mail: lfyan@ustc.edu.cn

† Electronic supplementary information (ESI) available. See DOI: https://doi.org/10.1039/d4gc02083a

This journal is © The Royal Society of Chemistry 2024

Published on 27 2024. Downloaded on 14/05/2026 05:56:35.

Although there are quite a few systems for dissolving cellulose, most of them have disadvantages such as high cost, poor stability, and non-environmental friendliness.[34,35] Compared to other solvents, ILs have been proved to be one of the most promising solvents due to their unique physicochemical properties such as low vapor pressure, high chemical and thermal stability, excellent solvency, and ease of recovery.[36,37] More importantly, ILs are structurally designable, which allows ILs to achieve desired properties by changing the structure of anions and cations.

As early as 2002, 1-*N*-butyl-3-methylimidazolium chloride ([C_4mim] Cl) IL was first used to efficiently dissolve cellulose.[31] Since then, the field of cellulose dissolution using ILs has been enriched and developed. Subsequently, Rogers and Zhang *et al.* reported that 1-*N*-allyl-3-methylimidazolium chloride ([Amim]Cl) IL is a powerful solvent for cellulose, and MCC can be dissolved rapidly without any treatments.[31,38] The team also noted that 1-*N*-ethyl-3-methylimidazolium acetate ([C_2mim] [CH_3COO]) IL, which has a small viscosity and melting point, exhibits a greater ability to dissolve cellulose. In addition, Ohno *et al.* found that *N*,*N*′-dialkylimidazolium formates ([RR′im] [HCOO]) and *N*-ethyl-*N*′-methylimidazolium alkyl phosphates ([C_2mim] [$(MeO)_2PO_2$]) ILs have excellent solubility for cellulose.[59] Referring to the published works, Xu *et al.* prepared 22 imidazolium-based ILs for dissolving cellulose, which greatly enriched the solvent systems for cellulose, and the cellulose solution can be used to prepare porous cellulose materials.[40] Recently, Zheng *et al.* utilized 1-butyl-3-methylimidazolium chloride ([Bmim][Cl]), 1-allyl-3-methylimidazolium chloride ([Amim][Cl]) and 1-ethyl-3-methylimidazolium acetate ([Emim][Ac]) ILs to efficiently dissolve cellulose and prepare regenerated cellulose films with high crystallinity, transparency, and tensile strength.[41]

Analysing the cellulose solvent systems mentioned above, it is evident that the solvent systems are concentrated on imidazolium-based ILs. Although the solubility is excellent, the strong interactions between anions and cations in imidazolium-based ILs result in higher viscosity.[42] This means that complete dissolution of cellulose usually requires longer mixing times, higher temperatures, and more vigorous mechanical agitation, which in turn can lead to the degradation of the solvent and cellulose.[43] In addition, imidazolium-based ILs typically require multi-step synthesis and purification and are relatively expensive.[44–46] In order to solve these problems, the exploration of novel ILs, which have not only low viscosity and high cellulose solubility but also simple synthesis conditions, is of great significance and value for the processing and application of cellulosic materials.

Similar to DESs, protonic ionic liquids (PILs) are a class of solvents prepared from a mixture of proton acids and proton bases. Unlike imidazolium-based ILs, PILs are diverse, simple, and inexpensive to prepare, and have been widely used in green catalysis and materials.[47–49] In general, proton bases mainly include 1,8-diazabicyclo [5.4.0] undec-7-ene (DBU), 1,5-diazabicyclo [4.3.0] non-5-ene (DBN), 7-methyl-1,5,7-triazabicyclo [4.4.0] dec-5-ene (TBD), and 1,1,3,3-tetramethylguanidine (TMG), which exhibit high hydrogen bonding alkalinity.[50] Proton acids, which mainly include organic monoacids such as formic acid, acetic acid, propionic acid, acetyl propionic acid, and acrylic acid, have high hydrogen bonding acidity and readily combine with proton bases to form homogeneous and transparent ILs.[47] Meenatchi *et al.* designed six PILs to replace imidazolium-based ILs, which could effectively dissolve cellulose.[51] For a comprehensive analysis of PILs, Li *et al.* designed 22 PILs to dissolve cellulose.[52] The results showed that the dissolution of cellulose was promoted by electron-donating groups, small space-site blocking groups, and short-chain groups in the proton acid anion and larger rings in the proton base cation. Moreover, the cellulose solutions were regenerated to prepare cellulose films with a high degree of polymerization, sufficient thermal stability, a smooth and dense surface, and high mechanical strength. Recently, Wang *et al.* designed a novel superbase-derived ionic liquid ([DBUH][$CH_3CH_2OCH_2COO$]) for dissolving cellulose and carried out a comprehensive analysis of the rheological properties of cellulose solution.[53] Ribeiro *et al.* used tetramethylguanidine-based ionic liquids to dissolve industrial cellulose pulp, and then cellulose films were also prepared by regeneration in a coagulation bath.[54] In addition, Deng *et al.* used levulinic acid-derived protic ionic liquids to simultaneously dissolve cellulose and wool keratin fibers and then obtained composite films by immersion in a coagulation bath, which had excellent mechanical properties, oxygen barrier properties, and thermal stability.[46]

Analyzing the current PILs, proton acids concentrate on liquid monoacids. The mechanism of ILs dissolving cellulose is the interaction of cations and anions, which disrupts the hydrogen bonding network in the cellulose molecular structure.[46,53] Therefore, diacids with high ionic strength become theoretical candidates for dissolving cellulose. Diacids are often solid, making them easier to stock and transport than liquid monoacids. Moreover, when liquid monoacids are mixed with proton bases they react immediately and generate a lot of heat, so operations such as ice baths, the passage of inert gases, and the addition of diluents are often required during the synthesis process, which significantly increases production costs.[52,53,55–57] However, when solid diacids are mixed with proton bases they do not react immediately, which shows their great advantage for industrial production. In addition, the currently prepared cellulose solution has a wide range of potential applications, which requires further research.[46,52–54,58]

In this work, eight superbase-derived ionic liquids (SILs) were prepared with superbases (DBN and DBU) and diacids (ethanedioic acid, malonic acid, succinic acid, and oxalic acid dihydrate), which could successfully dissolve microcrystalline cellulose and cotton wool. Analysing the solubility, it was clear that the molecular structures of the diacids and superbases were crucial for the solubility of cellulose. Moreover, the solvent was successfully recovered to repeat the dissolution of the cellulose. As shown in Scheme 1, cellulose solutions prepared with the new diacid–superbase ILs had excellent and versatile adhesion properties. In addition, the cellulose solutions

Published on 27 2024. Downloaded on 14/05/2026 05:56:35.

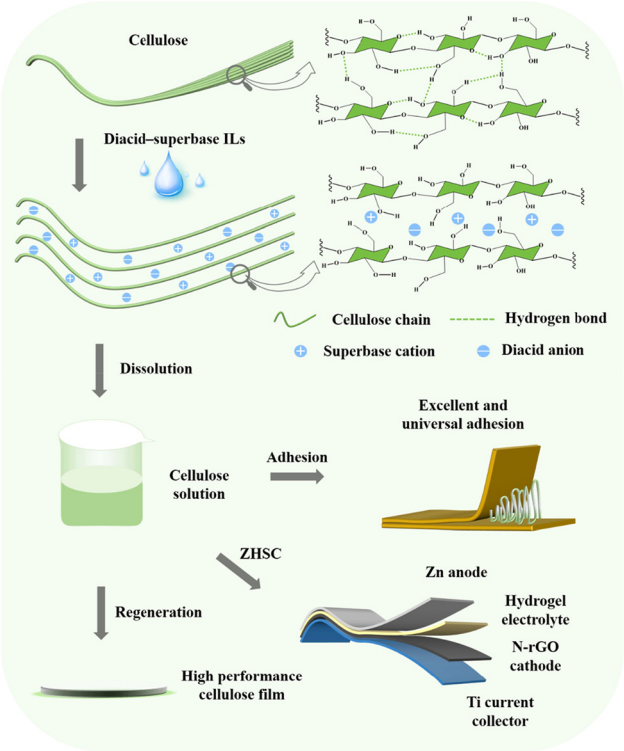

Scheme 1 Mechanism of cellulose dissolution by novel diacid–superbase ILs and preparation of the multifunctional cellulosic materials.

were regenerated through a coagulation bath to prepare cellulose films with structural integrity, dense morphology, high degree of crystallinity, excellent tensile strength (134 MPa), sufficient thermal stability, and excellent transparency. Finally, the cellulose gel regenerated by the coagulation bath was incorporated into a zinc-ion hybrid supercapacitor (ZHSC) with a wide voltage window, high energy and power densities, and excellent cycle life.

Results and discussion

Characterization of the SILs

The superbase has a strong ability to capture protons, which in turn means that it easily forms cations. The diacid has two carboxyl groups and can lose two protons to form anions. Therefore, the molar ratio of the superbase to the diacid was fixed at 2 : 1, and then the transparent and homogeneous liquid was obtained by heating and stirring (Fig. 1a). What's more, unlike monoacids, diacids are solid. Diacids do not generate a lot of heat and produce volatiles when they are mixed with a liquid superbase. Therefore, the prepared diacid solvent system is more favourable for industrial production, greatly reducing the equipment requirements and production costs.

Eight SILs (Fig. S1†) were prepared using superbases (DBU and DBN) and diacids (ethanedioic acid, malonic acid, succinic acid, and oxalic acid dihydrate). It can be noticed that only DBN-Ma and DBU-Ma presented a liquid state at room temperature, while the other SILs solidified or crystallized. In order to study the interactions between solvents, the solvents were characterized by ^{1}H NMR spectroscopy using DBN-Ma and DBU-Ma as templates (Fig. 1b). It was clearly seen that the proton signal on the carboxyl group in the diacid disappeared because the superbase captured the protons, which proved the formation of anions and cations in the solvent. In addition, the proton signals of both DBN-Ma and DBU-Ma were shifted to a lower field compared to the superbases (DBN and DBU), which was attributed to the formation of anions and cations that reduced the density of the extranuclear electron cloud around the superbases' protons.[35] In conclusion, the formation of anions and cations and the alteration of proton signals in the solvents contributed to the disruption of hydrogen bonding interaction between the cellulose molecular chains and promoted cellulose dissolution.[35]

Dissolution of cellulose in the SILs

To evaluate the ability of SILs to dissolve cellulose, MCC (DP = 260) and cotton wool (DP = 685) were used as templates for the study. As shown in Fig. S3,† MCC and cotton wool showed the short rod shapeand long fibrous shape under a microscope due to the different lengths of cellulose molecular chains caused by the different DPs. After SIL treatment, the short rod shape and long fibrous shape disappeared, which proved the dissolution of cellulose.

The dissolving ability of SILs for MCC is shown in Table S1† and Fig. 1c. It can be seen that the solubility of MCC in both DBN and DBU systems showed the following trend: malonic acid > ethanedioic acid > succinic acid > oxalic acid dihydrate. The malonic acid system had the best solubility for MCC, which was mainly attributed to the special molecular structure of malonic acid. Previous studies showed that the presence of both electron-donating groups and smaller space-site resistance groups on the anion promoted cellulose dissolution.[52] Due to the conjugation effect, the electron cloud of the ethanedioic acid anion is biased towards the middle of the molecule, resulting in weakened electronegativity. The malonic acid anion and succinic acid anion do not have a conjugation effect, but the molecular structure of the succinic acid anion is larger and the site-blocking effect is more significant, which is unfavorable for dissolution. In addition, the cellulose structural unit consists of the hydrophobic alkyl ring and the hydrophilic hydroxyl group, while the presence of the hydrophilic carboxyl anion and the hydrophobic methylene group in the malonic acid anion is more favorable for affinity with cellulose, thus promoting dissolution. However, in the oxalic acid dihydrate system, the presence of a small amount of water hinders the interaction between the ions and the cellulose molecules, leading to a significant decrease in solubility.

It can also be seen that the superbase (DBU) with a larger ring is more favorable for dissolution, which is consistent with previous studies.[52] The ability of the solvent to dissolve cellulose can be evaluated on the basis of the empirical Kamlet–Taft parameter of the solvent and the ability of the solvent to dissolve cellulose is positively correlated with the β

 This journal is © The Royal Society of Chemistry 2024

Published on 27 2024. Downloaded on 14/05/2026 05:56:35.

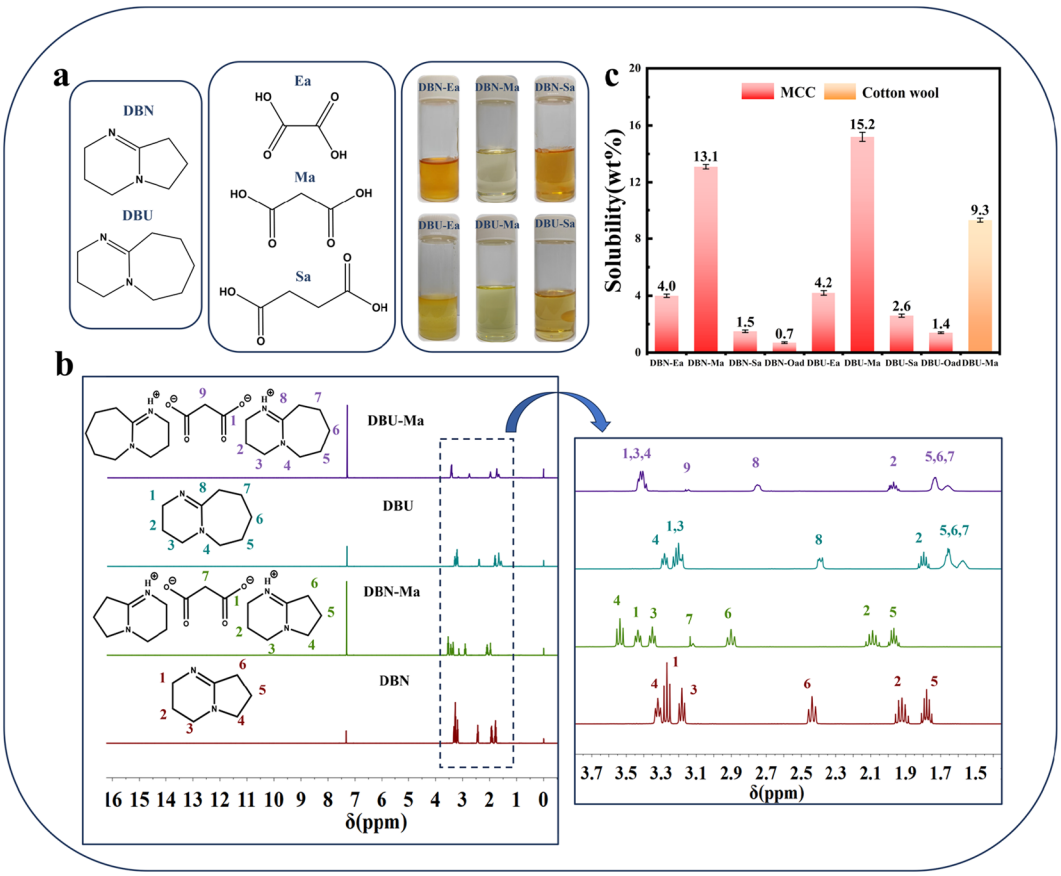

Fig. 1 The composition and photographs of SILs (a), ^{1}H NMR spectra of DBN-Ma and DBU-Ma (b), and the solubility of cellulose by different SILs (c).

parameter.[52,59] To achieve cellulose dissolution, the β parameter is greater than 0.80 and the β–α parameter is in the range of 0.35–0.90.[52] Because DBN-Ma and DBU-Ma were in a liquid state at room temperature, the Kamlet–Taft parameters of these two systems were determined as shown in Table S2.† It can be clearly seen that the β parameter was greater than 0.80 and the β–α parameter was in the range of 0.35–0.90. In addition, the β parameter and β–α parameter of DBU-Ma were greater than those of DBN-Ma, so DBU-Ma showed a better dissolving ability.

Meanwhile, in order to investigate the ability of SILs to dissolve cellulose of greater DP, the DBU-Ma system was used to dissolve cotton wool (DP = 685). For MCC (DP = 260), DBU-Ma can dissolve 15.2 wt%. As the DP increases, the cellulose molecular chain grows, so a larger spatial site resistance exists to resist dissolution.[35,54] Although the DP of cotton wool was as high as 685, DBU-Ma can still dissolve 9.3 wt% of cotton wool. As a result, the designed novel diacid–superbase ionic liquids are able to dissolve cellulose over a wide range of DPs, which greatly extends their industrial applications. As shown in Table S4,† comparing this work with that on other solvents, it can be seen that diacid–superbase ILs are better than most solvents.

In order to study the interaction between cellulose and solvent during dissolution, ^{1}H NMR analysis was conducted on DBU-Ma dissolved with 10 wt% of cellobiose. As shown in Fig. S4,† it was evident that the carboxyl signal that disappeared in the original DBU-Ma reappeared. This was attributed to the fact that due to the dissolution of cellobiose, a new strong hydrogen bond was formed between the affinity site of the cellobiose and the malonic acid anion, aligning with previous studies.[35] Furthermore, the dissolution process was driven by the formation of hydrogen bonds between the solvent and the cellulose.[35] As a result, the chemical shifts of the proton peaks were changed to varying degrees. Based on the above content, the mechanism of cellulose dissolution by SILs was analyzed as shown in Fig. S5.†[35,46,53] Superbases and diacids are mixed at high temperatures to form superbase cations and diacid anions, respectively. Under high temperature and stirring conditions, anions and cations penetrate between the cellulose molecular chains. The superbase cations and the diacid anions form hydrogen bonds with the oxygen and hydrogen atoms in the cellulose molecular chains, destroying the original hydrogen bonding network of the cellulose and thus achieving dissolution.

Currently, none of the reported monoacid SILs mention solvent recovery.[35,51–53] In this study, the solvent recovery of SILs is discussed using DBU-Ma as a template for the first time. The specific pathway for solvent recovery is shown in

Published on 27 2024. Downloaded on 14/05/2026 05:56:35.

Scheme S1.† An anti-solvent (anhydrous ethanol) was added to DBU-Ma of 2 wt% MCC, and then the recovered DBU-Ma was obtained by filtration and distillation under reduced pressure, which was used to repeatedly dissolve MCC. It was worth noting that the anti-solvent was anhydrous ethanol instead of deionized water, and the boiling point of anhydrous ethanol was much lower than that of deionized water, which meant that this would significantly reduce energy consumption and promote sustainable development. DBU-Ma was recycled three times and pictures of the the recycled DBU-Ma are shown in Fig. S6.† After three cycles, the dissolution of the MCC was still achieved (Fig. S7†). Moreover, the ^{1}H NMR spectra of the recovered and fresh DBU-Ma were analyzed (Fig. S6†). The spectra clearly showed that the proton signals of the recycled DBU-Ma were very similar to those of the fresh DBU-Ma, which showed that the dissolution of MCC could still be achieved by the recycled DBU-Ma after several cycles. However, the ability of the recovered DBU-Ma to dissolve cellulose was reduced due to the addition of water and impurities (Fig. S6†).

The rheological properties of cellulose solutions

In the preparation of cellulosic materials, the rheological properties of the cellulose solution are crucial for establishing the process parameters.[56,60,61] Therefore, the DBU-Ma system was used as a template to study the rheological properties of cellulose solutions with different concentrations in this work (Fig. 2a). The relationship between viscosity and temperature for cellulose solutions with different concentrations is shown

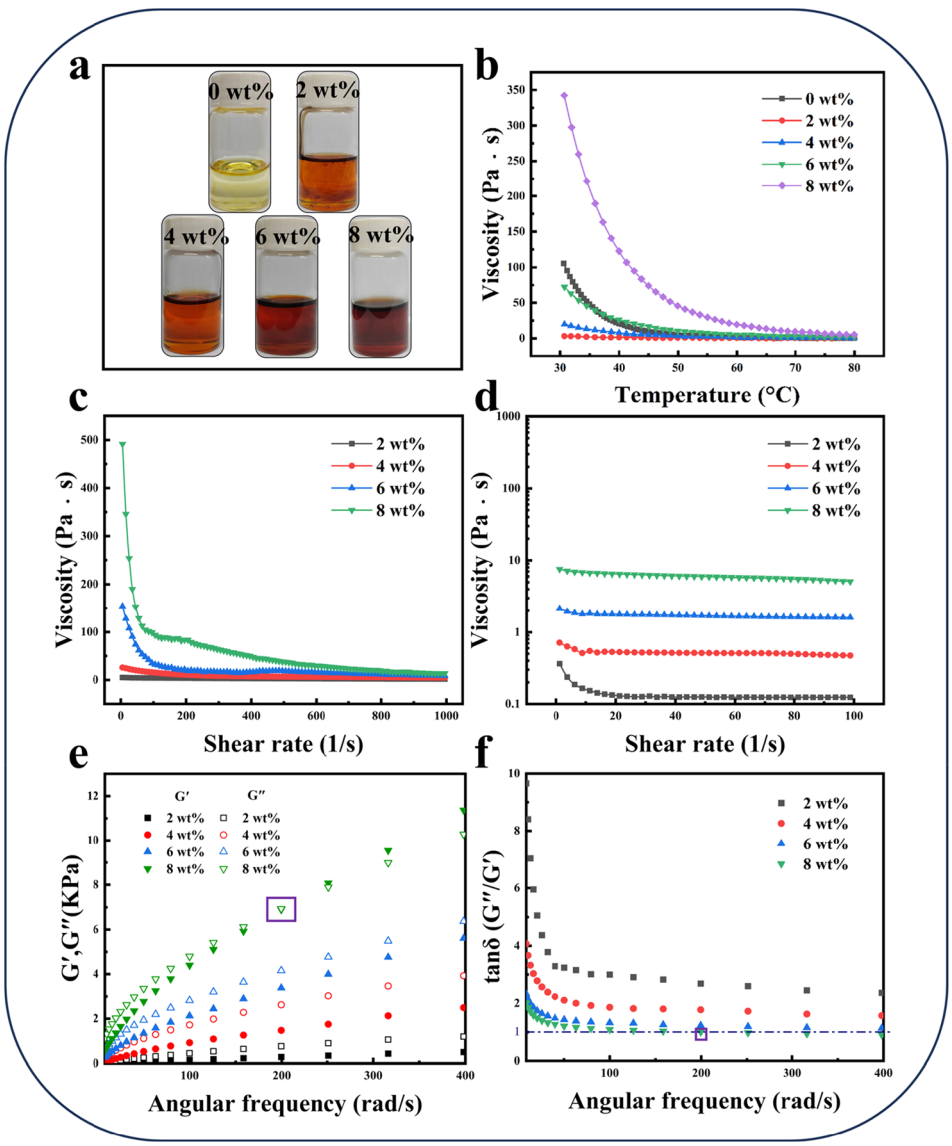

Fig. 2 Photographs of cellulose solutions with different concentrations (a), the relationship between viscosity and temperature for cellulose solutions with different concentrations (b), the relationship between viscosity and shear rate for cellulose solutions with different concentrations at room temperature (c) and 80 °C (d), and the dependence of G', G'' and tan δ on ω of cellulose solutions with different concentrations at room temperature (e and f).

This journal is © The Royal Society of Chemistry 2024

Published on 27 2024. Downloaded on 14/05/2026 05:56:35.

in Fig. 2b. It was found that the viscosity was highly correlated with the concentrations of cellulose, with a higher cellulose concentration resulting in higher viscosity at 30 °C. The viscosity value increased from 3.114 Pa s to 342.708 Pa s when the concentration of cellulose increased from 2 wt% to 8 wt% at 30 °C. However, the viscosity value of the pure solvent was high (105.292 Pa s at 30 °C), which was attributed to the strong electrostatic interaction formed between the malonic acid anion and the DBU cation. As the temperature increased, the viscosity of cellulose solutions with different concentrations decreased until it became stable. This was because as the temperature increased, the thermal movement of the molecules in the solution accelerated, reducing the interaction between the molecules. These results indicate that the viscosity of cellulose solutions of appropriate concentration is less than that of pure solvent, and increasing the temperature can also significantly reduce the viscosity of cellulose solutions. Therefore, choosing a cellulose solution of appropriate concentration and increasing the temperature are essential for the conversion and processing of cellulose.[53]

The relationship between viscosity and shear rate for cellulose solutions with different concentrations at room temperature is shown in Fig. 2c. At 0 shear rate, the viscosity of the cellulose solution increased with increasing concentration, which responded to the enhanced interaction between cellulose and solvent molecules.[53] In addition, cellulose solutions with different concentrations showed a typical shear-thinning behavior, which was the constant decrease of the viscosity value as the shear rate increased. This was attributed to the orientation of the cellulose molecular chains in the direction of flow under shear stress, leading to the reduction of viscosity.[53] Moreover, when the shear rate exceeded 200 1 s^{-1}, the cellulose chains of bonding or aggregation structure were completely unwound and oriented, and the viscosity value of the solution was kept stable.[60,62] Similar results were reported in other polymer solutions.[56,63,64] At 80 °C, the relationship between viscosity and shear rate for cellulose solutions with different concentrations was also analyzed (Fig. 2d). At 80 °C, the cellulose solutions all showed very low viscosity values (below 10 Pa s). Similar to the room temperature situation, the cellulose solutions still showed the typical shear-thinning behavior, with the viscosity value remaining constant at a shear rate above 10 1 s^{-1}.

The dependence of the energy storage modulus (G') and loss modulus (G'') on the angular frequency (ω) of cellulose solutions with different concentrations at room temperature was further investigated, as shown in Fig. 2e. It can be seen that when the concentration of cellulose was lower than 6 wt%, the value of G' was always smaller than the value of G'' in the measured angular frequency range, which indicated that the system presented the characteristics of the viscous liquid. In this situation, most of the energy was dissipated through the viscous flow because the deformation of the solution changed very slowly.[53] However, when the concentration of cellulose was 8 wt%, G' increased more rapidly with increasing angular frequency, resulting in the G' and G'' curves intersecting, which indicated a transition of the system from a viscous liquid to an elastic solid. At this point, the entangled network structure in the solution was in a steady state, which caused the solution to exhibit the characteristics of an elastic solid.[65] In addition, the viscoelasticity of the cellulose solutions can be described by the loss angle tangent ($\tan\delta$), as shown in Fig. 2f. The $\tan\delta$ values of cellulose solutions with different concentrations decreased gradually with increasing angular frequency, which indicated that the solutions showed a liquid–solid transition trend. When the concentration of cellulose was 8 wt%, the cross point of the dynamic modulus (COP) appeared around 200 rad s^{-1} and 6900 Pa, whereas other cellulose solutions did not have a COP. The above results indicated that the interaction between cellulose molecules was significantly enhanced as the concentration of cellulose was increased, which was more conducive for the transformation of the system to an elastic solid.

In summary, the rheological properties of cellulose solutions were analyzed in detail, providing important parametric information for film casting and fiber spinning. In this work, the excellent viscoelastic properties of cellulose solutions contribute to fiber spinning. Viscosity is a factor to be considered in the preparation of different cellulosic materials.[53] This is because high-viscosity systems are difficult to handle, require a lot of energy, and can cause discontinuities in the film-casting process. Low-viscosity systems are easy to produce but do not improve the required viscoelasticity in fiber spinning. Therefore, for the preparation of different cellulosic materials, the corresponding solution viscosity needs to be selected for successful industrial production.

The adhesion properties of cellulose solutions

As shown in Fig. S1,† the six SILs (except DBN-Ma and DBU-Ma) were in a solid state at room temperature and transformed into a highly adhesive liquid state at high temperature, which gave them the potential to be adhesives. In this study, the adhesive properties of cellulose solutions were investigated using the DBU-Ea system as a template.

As shown in Fig. 3a, the cellulose solutions with different concentrations (0 wt%, 2 wt%, and 4 wt%) were in a solid state at room temperature and presented a flowing liquid state at 100 °C. To evaluate the adhesive properties, the cellulose solutions were coated on wood panels and tested for tensile properties by hot-pressing at 100 °C after cooling to room temperature (Fig. 3b). As shown in Fig. 3c, the tensile strength of the pure DBU-Ea solvent reached 1.64 MPa, which was attributed to the strong electrostatic interaction between the superbase cation and the ethanedioic acid anion. The tensile strength increased gradually with increasing cellulose concentration. The tensile strength of the 4 wt% cellulose solution reached 2.39 MPa, which was attributed to the enhanced interaction and entanglement of the cellulose molecular chains, leading to increased cohesive strength. In addition, the surface of the wood panel coated with the solution was analyzed by SEM (Fig. 3d). It can be clearly seen that there were many tiny air holes and large pores on the surface of the original wood

Published on 27 2024. Downloaded on 14/05/2026 05:56:35.

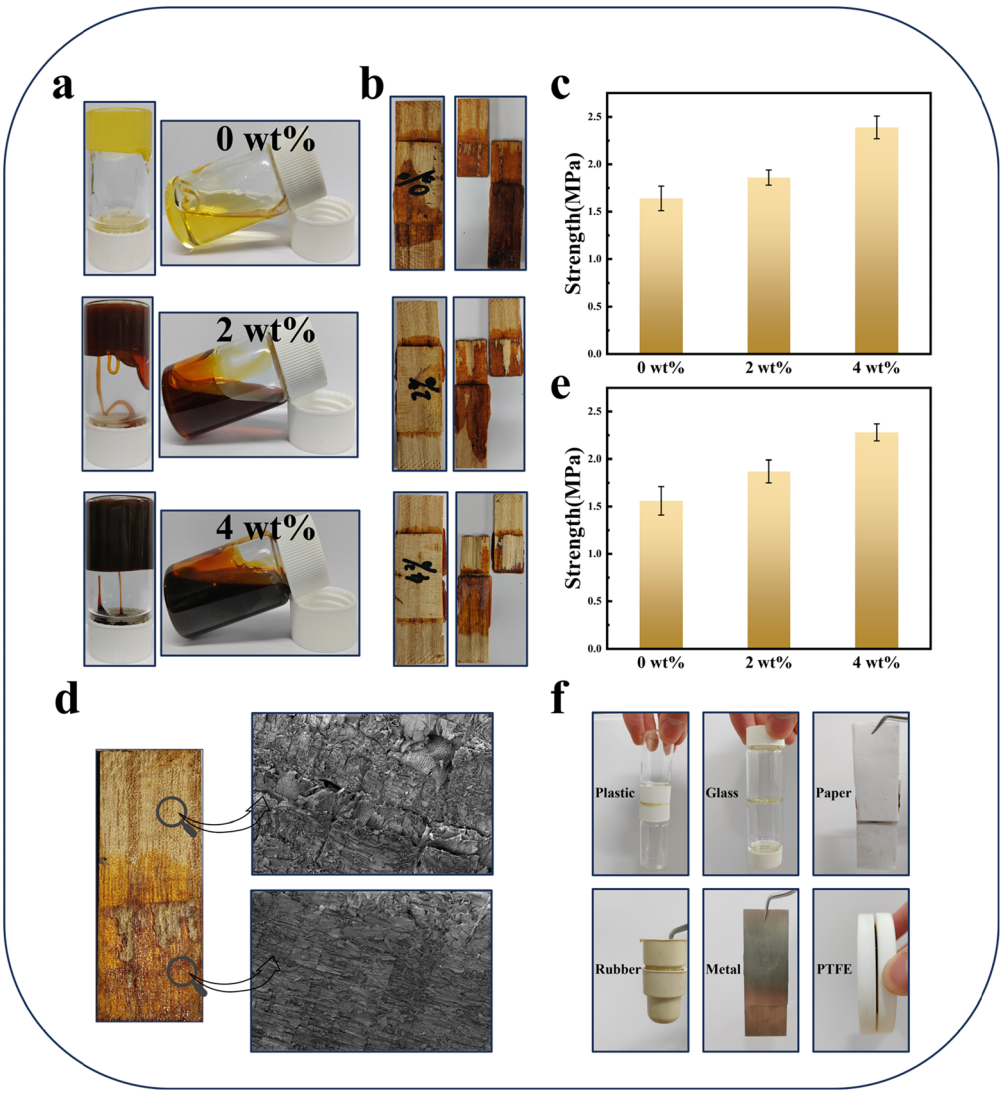

Fig. 3 Photographs of the cellulose solutions with different concentrations at room temperature (left) and 100 °C (right) (a), the photographs of the adhesion of cellulose solutions to wood panels (b), the tensile strength of wood panels by cellulose solutions (c), the SEM photographs of the surface of the wood panel (d), the tensile strength of bamboo panels by cellulose solutions (e), and photographs of the adhesion of cellulose solutions to different substrates (f).

panel. However, the air holes and pores of the wood panel disappeared after hot-pressing, which indicated that the solution penetrated the interior of the wood panel very easily under high-temperature conditions, further increasing the tensile strength.

Moreover, the tensile strength of the cellulose solution for the bamboo panel was also determined under the same conditions, and the results are shown in Fig. 3e. Similar to the test results of the wood panel, the tensile strength gradually increased with increasing cellulose concentration. The tensile strength of the 4 wt% cellulose solution reached 2.28 MPa, which demonstrated that the prepared cellulose solution had universal and high adhesion properties to the plates. To further demonstrate the universal and adaptive adhesion properties of the cellulose solution, a variety of substrates (plastic, glass, paper, rubber, metal, and PTFE) could be tightly adhered as shown in Fig. 3f. In summary, cellulose solution had universal and strong adhesion properties, which were attributed to the fact that the system could form attractive interactions with polar groups on the substrates such as hydrogen bonding, electrostatic attraction, ion–dipole interaction, and coordination bonding (Fig. S10†).[66]

Characterization of cellulose films

Regenerated cellulose was obtained by adding an anti-solvent (95% ethanol solution) to cellulose solutions with different concentrations. Because of the growing concentration of cellulose, the dissolving time increased accordingly, leading to increased degradation of the ionic liquid and cellulose

 This journal is © The Royal Society of Chemistry 2024

Published on 27 2024. Downloaded on 14/05/2026 05:56:35.

(Table S3 and Fig. S11†). As a result, the regenerated cellulose deepened in color and decreased in the DP (Fig. S11†).

The cellulose films were prepared by cellulose solutions as shown in Fig. 4a. By placing the films on top of the white paper corresponding to the concentration, the number can be clearly seen through the films. Moreover, the light transmittance of the cellulose films was determined by UV analysis (Fig. 4d). As the concentration of cellulose increased, the light transmittance of the cellulose films became worse. However, the light transmittance of cellulose films with different concentrations was above 50% in the visible region. In addition, cellulose films can be bent arbitrarily without rupture and exhibit good toughness (Fig. 4a). Meanwhile, SEM showed that the surface of the cellulose films was dense and smooth, with no holes and folds (Fig. 4b). It was worth noting that as the concentration of cellulose increased, some of the cellulose chains agglomerated, so microspheres appeared on the surface of the cellulose films.

To evaluate the mechanical properties of cellulose films, the cellulose films were tested for tensile properties. As shown in Fig. 4c, the tensile strength of the films gradually increased with increasing cellulose concentration. The maximum tensile

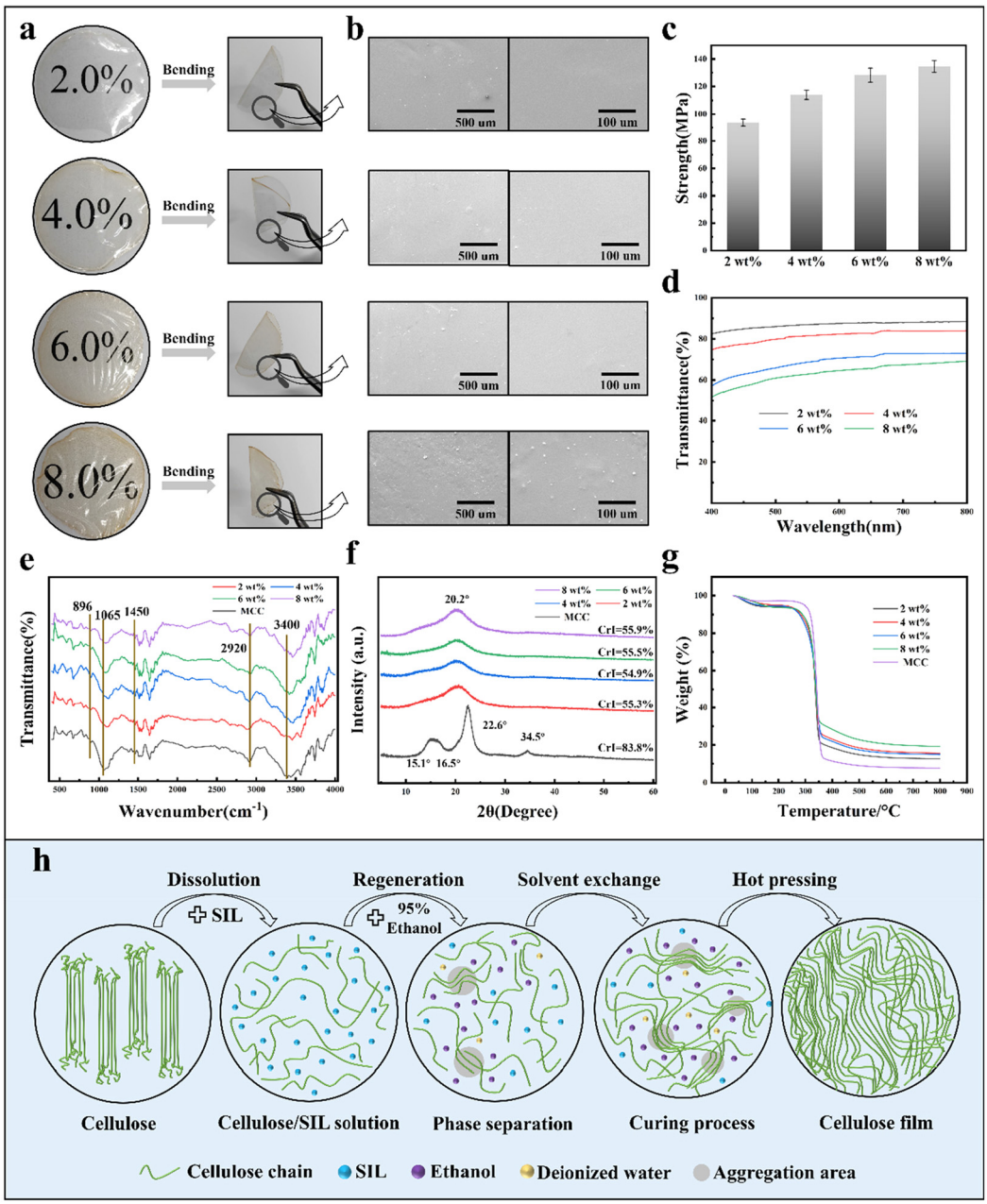

Fig. 4 Photographs (a), SEM photographs (b), tensile strength (c), transmittance (d), FTIR spectra (e), XRD spectra (f), and TG curves (g) of cellulose films with different concentrations, and the microstructural evolution of cellulose films during dissolution and regeneration processes (h).

Published on 27 2024. Downloaded on 14/05/2026 05:56:35.

strength of the cellulose film was 134.47 MPa when the concentration of cellulose was 8 wt%. Further analysis of the stress–strain curves showed that the tensile strength of the films gradually increased with increasing cellulose concentration, but the elongation at break gradually decreased (Fig. S12†). This was attributed to the fact that the greater the cellulose concentration, the denser the cellulose molecular chains were in the same spatial range, leading to enhanced interaction of cellulose molecular chains and increased cohesive strength. However, the greater the concentration of cellulose, the tighter the fibers were stacked and the less flexible the molecular chains became, leading to a decrease in elongation at break.

The FTIR spectra of MCC and cellulose films are shown in Fig. 4e. The FTIR spectra of cellulose films with different concentrations were very similar to those of MCC, indicating that the molecular structure of cellulose was not destroyed during the dissolution and regeneration process.[38] The FTIR spectra included 896, 1065, 1450, 2920, and 3400 cm^{-1} typical cellulose characteristic peaks corresponding to β-1,4-glycosidic bond vibration, C–O–C stretching vibration, C–H bending vibration, C–H stretching vibration, and O–H stretching vibration, respectively.[67–69] Notably, both the C–O–C and O–H stretching vibrations of the cellulose films were redshifted to different degrees, suggesting that the hydrogen bonding network of the original cellulose was disrupted and the cellulose molecular chains were reorganized in the process of regeneration.[52,70] The FTIR results showed that the cellulose films only underwent the crystalline phase transition without accompanying changes in the chemical structure.

The crystalline structures of MCC and cellulose films were investigated by XRD characterization as shown in Fig. 4f. MCC was a cellulose I structure with diffraction peaks at 2θ = 15.1, 16.5, 22.6 and 34.5°, corresponding to the $(11\bar{0})$, (110), (200), and (004) crystal planes.[39,71] The cellulose films were completely transformed from cellulose I structure to cellulose II structure with the presence of the diffraction peak at 2θ = 20.2°, corresponding to the (110) crystal plane.[35] The crystallinity (CrI) of cellulose was calculated by referring to the published work.[72] The CrI values of cellulose films with different concentrations (2 wt%, 4 wt%, 6 wt%, and 8 wt%) were 55.3%, 54.9%, 55.5%, and 55.9%, which were less than the CrI of MCC (83.8%). The above results indicated that during the dissolution of cellulose, intermolecular and intramolecular hydrogen bonds were disrupted, resulting in the destruction of the original cellulose I structure and the cellulose aggregate into the form of a single molecular chain. Then in the coagulation bath (95% ethanol solution), the cellulose molecular chains were restructured and the cellulose II structure with low crystallinity was formed.[52] The above results corresponded to the FTIR results.

The thermal stability behavior of cellulose films and MCC at different temperatures was investigated using thermogravimetric analysis (Fig. 4g and Fig. S13†). From the TG curves, it can be seen that cellulose films with different concentrations and MCC had similar shapes, indicating that the structure of the cellulose films remained intact. It was clear from the curves that the weight loss was divided into two stages.[46] The first stage was the volatilization of water (0–150 °C) and the second stage was the decomposition of cellulose (230–400 °C). It was worth noting that the initial and maximum decomposition temperatures of MCC were 260 °C and 386 °C, respectively. In contrast, the initial and maximum decomposition temperatures of cellulose films were in the ranges of 230–250 °C and 373–378 °C, both of which were lower than those of MCC. This was due to a certain degree of degradation of MCC during the dissolution process, with a decrease in the DP and the shortening of the molecular chain. In addition, the thermal decomposition residues (non-volatile carbonaceous substances) of cellulose films (12.6–19.2%) were higher than those of MCC (7.7%), which was consistent with previous work.[53] Overall, the cellulose films still maintained excellent thermal stability, undergoing crystalline phase transition during dissolution and regeneration without structural changes, which corresponded well with the XRD and FTIR results.

In order to clarify the preparation mechanism of high-performance cellulose films, the microstructural evolution of cellulose during dissolution and regeneration was discussed in conjunction with the above analysis, as shown in Fig. 4h.[53] The structure of MCC consists of crystalline and amorphous regions. The crystalline region is formed by the close arrangement of cellulose molecular chains through the interaction of intramolecular and intermolecular hydrogen bonds. At high temperatures, the superbase cations and the diacid anions break the hydrogen bonding network in the cellulose molecular chain and form a new hydrogen bonding network with the cellulose molecular chain, which achieves the dissolution of the cellulose and obtains a transparent and homogeneous liquid. The addition of the anti-solvent (95% anhydrous ethanol) to the cellulose solution enables the formation of a macroscopic continuous state by the re-aggregation of the cellulose molecular chains. When the anti-solvent is added to the cellulose solution, there is immediate solvent exchange and phase separation due to the changing ratio of cellulose molecular chains, SIL and anti-solvent. In this process, water molecules mainly act as hydrogen bond donors interacting with diacid anions, while ethanol molecules mainly act as hydrogen bond acceptors interacting with superbase cations.[53,73,74] In addition, due to the concentration difference, water and ethanol molecules can continuously diffuse into the cellulose solution. As a result, the curing process occurs due to the continuous aggregation of cellulose molecular chains. Finally, cellulose films with structural integrity, dense morphology, high degree of crystallinity, excellent tensile strength, sufficient thermal stability, and excellent transparency are prepared by hot-pressing.

Zinc-ion hybrid supercapacitor (ZHSC)

The cathode (N-rGO on the Ti current collector), anode (Zn foil as the anode material and current collector), and cellulose gel soaked in 2M $ZnSO_4$ as the electrolyte were assembled to form

 This journal is © The Royal Society of Chemistry 2024

Published on 27 2024. Downloaded on 14/05/2026 05:56:35.

the ZHSCs (Fig. 5a and Fig. S14†). The strength of 2 wt% cellulose gel was too low to be used as a solid electrolyte for assembling ZHSCs. Therefore, the ZHSCs prepared with 4 wt% and 6 wt% cellulose gels were named ZHSC-4 and ZHSC-6, respectively. As shown in Fig. 5b–e, the electrochemical properties of ZHSC-4 and ZHSC-6 were measured by cyclic voltammetry (CV) and galvanostatic charge–discharge technique (GCD). Both the ZHSC-4 and ZHSC-6 CV curves showed a quasi-rectangular shape with a small peak due to the battery-type anode when the scan rates were 2, 5, 10, 20, and 50 mV s^{-1}. Moreover, a wide voltage window of 2 V was achieved for both ZHSC-4 and ZHSC-6. The GCD curves of ZHSC-4 and ZHSC-6 showed a quasi-triangular and symmetric shape in the range of current density from 0.5 to 10 A g^{-1}, suggesting that the electric double-layer capacitor-type behavior was dominant.[75] However, it can be clearly seen that the CV curve of ZHSC-4 constituted a larger area than that of ZHSC-6 while the GCD curve of ZHSC-4 was slower than that of ZHSC-6, indicates ZHSC-4 is better than ZHSC-6 (Fig. S16†).[76] In addition, the impedance data of ZHSC-4 and ZHSC-6 were measured, as

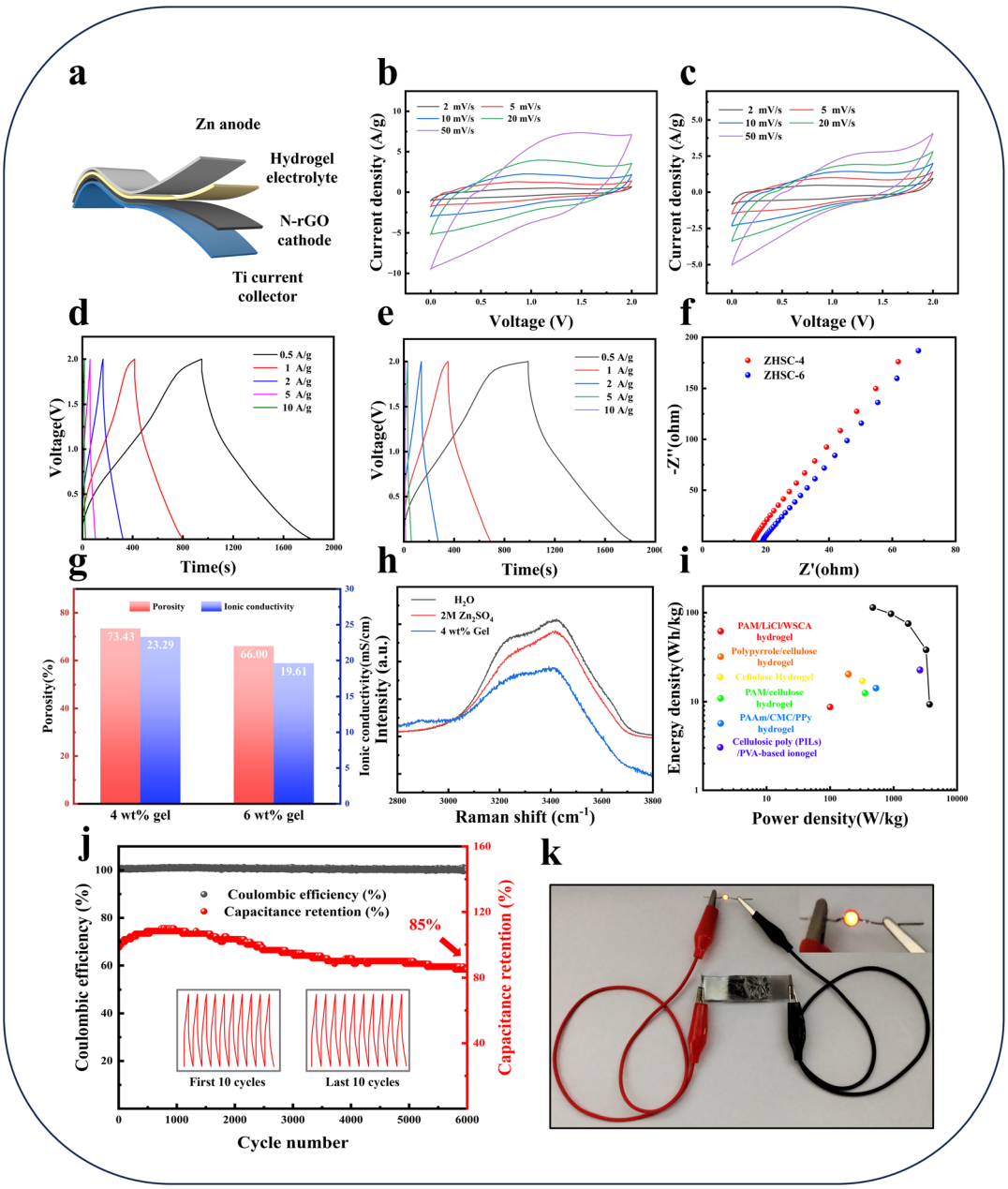

Fig. 5 The component model of ZHSC (a), CV curves of ZHSC-4 (b) and ZHSC-6 (c), GCD curves of ZHSC-4 (d) and ZHSC-6 (e), the impedance plots of ZHSC-4 and ZHSC-6 (f), the porosity and ionic conductivity of 4 wt% and 6 wt% gels (g), Raman spectra of H_2O, 2 M H_2SO_4 and 4 wt% gel (h), Ragone plot of ZHSC-4 with the reported devices (i), the capacitance retention and coulombic efficiency of ZHSC-4 at 10 A g^{-1} during 6000 cycles (j), and a photograph of a small bulb lit up by ZHSC-4 (k).

Published on 27 2024. Downloaded on 14/05/2026 05:56:35.

shown in Fig. 5f. After conversion, the ionic conductivities of ZHSC-4 and ZHSC-6 were 23.29 mS cm^{-1} and 19.61 mS cm^{-1}, which explained the superior electrochemical performance of ZHSC-4.[76] To further explain the difference in electrochemical properties of ZHSC-4 and ZHSC-6, porosity measurement and SEM analysis of 4 wt% and 6 wt% cellulose gels were carried out (Fig. 5g and Fig. S17†). It can be clearly seen that the porosity and microscopic pore size of the 4 wt% cellulose gel were greater than those of the 6 wt% cellulose gel, which was attributed to the high concentration of cellulose resulting in tightness between the fibers and reduced pore size. Therefore, the increase in porosity and pore size facilitated the transport of ions, which increased the ionic conductivity and capacitance, resulting in the superior electrochemical performance of ZHSC-4.[77,78]

As shown in Fig. 5h, in order to investigate the form of water molecules in the gel electrolyte, Raman analysis was carried out. In 2M Zn_2SO_4 aqueous solution, the structure of the hydrogen bonding network between water molecules was destroyed, and a new interaction between Zn^{2+} and water molecules was formed, which limited the vibration of water molecules and decreased the intensity of Raman peaks. In cellulose gel, water molecules can interact not only with Zn^{2+} but also with hydroxyl functional groups in cellulose, causing the intensity of the Raman peak to decrease significantly and the position of the Raman peak to move in the direction of low wavenumbers. ZHSC-4 was further electrochemically characterized because of its excellent electrochemical properties. Energy density and power density are two important performance indicators for supercapacitors in practical applications. At 0.5 A g^{-1} current density, the energy density and power density of ZHSC-4 can reach 114.53 W h kg^{-1} and 470.78 W kg^{-1}, which are higher than the values for most of the reported cellulose hydrogel-based supercapacitors (Fig. 5i).[79–84] The service life is an important performance indicator for electric storage materials. Therefore, the performance of ZHSC-4 was tested for 6000 cycles at a current density of 10 A g^{-1}. As shown in Fig. 5j, the capacitance retention can still be maintained at 85% and the coulombic efficiency is close to 100% after 6000 charge/discharge cycles, which indicates that most of the charged ions in ZHSC-4 are involved in the discharging process and ZHSC-4 has a long lifetime.[79] Considering practical applications, the small bulb can be continuously lit when ZHSC-4 is fully charged (Fig. 5k). In summary, ZHSC-4 has a wide voltage window, high capacitance, energy density and power density, and excellent cycle life, so it had great potential for application in the field of electric storage.

Experimental

Materials

Microcrystalline cellulose (MCC) was purchased from YuanyeBio Company. Malonic acid, succinic acid, oxalic acid dihydrate, anhydrous ethanol, $ZnSO_4$, H_2SO_4, HCl, H_2O_2, potassium permanganate, and 4-nitroaniline were purchased from China National Pharmaceutical Group Chemical Reagent Co., Ltd. Copper(II) ethylenediamine was purchased from Energy Chemical Company. DBU, DBN, ethanedioic acid, and Nile red were purchased from ACMEC Company. Cellobiose was purchased from Macklin Company. Cotton wool was purchased from Hualu Company. Graphite powder was purchased from Alfa Aesar Company.

Preparation of SILs

Diacids (ethanedioic acid, malonic acid, succinic acid, oxalic acid dihydrate) and superbases (DBU and DBN) were added to a round-bottomed flask in a 1 : 2 molar ratio. The mixture was heated at 110 °C until it became a clear liquid and then stored in a desiccator for later use.

For the convenience of expression, the prepared SILs were named DBU/N-X, where X represents the type of diacid. Ethanedioic acid, malonic acid, succinic acid, and oxalic acid dihydrate were expressed as Ea, Ma, Sa, and Oad, respectively.

Dissolution of cellulose and recycling of SILs

A certain mass of SILs was weighed into a round-bottomed flask and then an appropriate amount of cellulose (MCC and skimmed cotton) was added to the flask. The mixture was stirred continuously at 100 °C until a clear solution was formed. All the dissolution experiments in this study were repeated three times under the same conditions. For the convenience of expression, the prepared cellulose solution was named DBU/N–X–Y, where X represents the type of diacid and Y represents the concentration of cellulose. For example, DBU-Ma-2% was expressed as a cellulose solution of 2 wt% DBU/malonic acid.

Using DBU-Ma as a template, cellulose was regenerated by adding the appropriate amount of anhydrous ethanol to the dissolution solution. The filtrate was obtained by filtration and the anhydrous ethanol was removed by distillation under reduced pressure to obtain recoverable SILs to repeat the cellulose dissolution. The SIL recovery scheme is shown in Scheme S1.†

Adhesion of cellulose solution to wood and bamboo panels

Cellulose solutions of different concentrations were coated onto the wood/bamboo panels and hot pressed at 100 °C for 5 h. The hot-pressed wood/bamboo panels were cooled at room temperature for the next step of testing.

Preparation of cellulose films

Cellulose solutions of different concentrations were coated in Petri dishes. Thin gels were obtained by soaking first in a coagulation bath of 95% anhydrous ethanol and then in deionized water to remove impurities. The prepared thin gels were hot pressed at 100 °C to obtain cellulose films.

Preparation of zinc-ion hybrid supercapacitor (ZHSC)

Cellulose solutions of different concentrations were poured into beakers. The gels were obtained by soaking first in a coagulation bath of 95% anhydrous ethanol and then in de-

 This journal is © The Royal Society of Chemistry 2024

Published on 27 2024. Downloaded on 14/05/2026 05:56:35.

ionized water to remove impurities. Then, the gels were placed in a 2 M $ZnSO_4$ solution for soaking. The N-rGO was prepared according to previous work.[85] The N-rGO was coated on the Ti network to form the cathode and zinc foil was used as the anode. Cellulose gel was sandwiched between the cathode and anode as an electrolyte to form ZHSC.

Optical microscopy test

Cellulose solution was dropped on a slide and the dissolution of cellulose was observed under the microscope.

Determination of KT parameters

Kamlet–Taft parameters (α, β, and π^*) were determined using 4-nitroaniline and Nile red (details are given in the ESI†).

Rheological properties test

The rheological properties of the cellulose solutions were tested using a rheometer (TA Discovery HR-2).

Fourier transform infrared (FT-IR) spectra characterization

FT-IR spectra were performed in the range of 400–4000 cm^{-1} using a Bruker Vector 2 spectrophotometer.

Nuclear magnetic resonance analysis

Deuterated chloroform was used as the solvent for ^1H NMR and ^{13}C NMR analysis (Bruker, Avance III, 400 MHz).

Characterization of the degree of polymerization (DP)

A viscometer was used to measure the DP of cellulose (details are given in the ESI†)

Thermal stability test

A thermogravimetric analysis test was performed under a N_2 environment (TGA Q5000 V3.17 Build 265 instrument). Cellulose was heated from 25 °C to 800 °C at a rate of 10 °C min^{-1}.

X-ray diffraction (XRD) characterization

Cellulose was characterized at diffraction angles ranging from 5° to 60° using a MiniFlex machine.

Film transparency test

The transmittance of the cellulose film in the visible light range (400–800 nm) was measured using a UV 1700PC ultraviolet–visible spectrophotometer.

Scanning electron microscopy (SEM) characterization

The microstructure of the cellulose film was observed using a GeminiSEM 500 machine.

Tensile property test

A universal testing machine (UTM2502) was used for the tensile test at room temperature.

Porosity determination

The average porosity of the gel was determined by the ethanol replacement method (details are given in the ESI†).

Raman spectroscopy test

The Raman spectrum of the sample was tested using a RAMAMLOG 6 (Spex, USA) with an excitation wavelength of 532 nm.

Determination of electrochemical properties

The electrochemical properties of ZHSC were tested using a CHI760E electrochemical workstation and LANHE.

Conclusions

In recent years, various monoacid-superbase ionic liquids have been used for the dissolution of cellulose. However, these systems have tended to concentrate on the study of cellulose dissolution, while the prepared cellulose solutions had only a single application. Inspired by these works, this work first prepared diacid–superbase ionic liquids for the efficient dissolution of cellulose. Unlike monoacids, solid diacids are mixed more gently with superbases, avoiding additional auxiliary operations. By comparing different types of diacids and superbases, DBU-Ma was found to have the best solubility for cellulose, which was attributed to the unique molecular structure of DBU and malonic acid. The final results showed that DBU-Ma could dissolve maximally 15.2 wt% of microcrystalline cellulose (DP = 260) and 9.3 wt% of cotton wool (DP = 685), which indicated that diacid–superbase ionic liquids were able to achieve cellulose dissolution over a wide range of DP values. For sustainable development, diacid–superbase ionic liquids can be successfully recycled to repeatedly dissolve cellulose. The rheological properties of cellulose solutions were analyzed to provide important parametric information for film casting and fiber spinning. Moreover, the cellulose solutions had excellent and universal adhesion properties and could achieve tensile strengths of 2.39 MPa and 2.28 MPa for wood and bamboo boards, respectively. In addition, cellulose solutions were regenerated in a coagulation bath and hot pressed to successfully prepare high-performance cellulose films with structural integrity, dense morphology, a high degree of crystallinity, excellent tensile strength (134 MPa), sufficient thermal stability, and excellent transparency. Finally, the gel prepared by cellulose solution was assembled into ZHSC with a wide voltage window (2 V), high energy density (114.53 W h kg^{-1}), and power density (470.78 W kg^{-1}). Moreover, the capacitance retention can still be maintained at 85% and the coulombic efficiency was close to 100% after 6000 charge/discharge cycles, which indicated that ZHSC had great potential for application in energy storage. In summary, the new diacid–superbase ionic liquids dissolve cellulose efficiently while solving the problem of the single application of cellulose solution, which opens up a feasible pathway for the conversion and application of cellulose.

Author contributions

Long Zhang carried out the experiments and wrote the manuscript, Boxiang Zhan, Yapeng He, Yongqi Deng, Haiyuan Ji and Shen Peng reviewed the literature, and Lifeng Yan designed, supported and wrote the paper.

Data availability

The data supporting this article have been included as part of the ESI.†

Conflicts of interest

There are no conflicts to declare.

Published on 27 2024. Downloaded on 14/05/2026 05:56:35.

Acknowledgements

This work is supported by the National Key R&D Program of China (No. 2023YFA1507500), the National Natural Science Foundation of China (No. 52373159), and the Fundamental Research Funds for the Central Universities (No. YD2060002015).

References

1 M. T. Clough, *Green Chem.*, 2017, **19**, 4754–4768.
2 A. R. Xu, X. Guo, Y. B. Zhang, Z. Y. Li and J. J. Wang, *Green Chem.*, 2017, **19**, 4067–4073.
3 E. J. Cho, L. T. P. Trinh, Y. Song, Y. G. Lee and H. J. Bae, *Bioresour. Technol.*, 2020, **298**, 122386.
4 T. Zhang, *Science*, 2020, **367**, 1305–1306.
5 D. Kaloudas, N. Pavlova and R. Penchovsky, *Environ. Chem. Lett.*, 2021, **19**, 2809–2824.
6 H. Tu, M. X. Zhu, B. Duan and L. N. Zhang, *Adv. Mater.*, 2021, **33**, 2000682.
7 M. B. Sticklen, *Nat. Rev. Genet.*, 2008, **9**, 433–443.
8 Y. Habibi, *Chem. Soc. Rev.*, 2014, **43**, 1519–1542.
9 X. F. Zhang, X. F. Ma, T. Hou, K. C. Guo, J. Y. Yin, Z. G. Wang, L. Shu, M. He and J. F. Yao, *Angew. Chem., Int. Ed.*, 2019, **58**, 7366–7370.
10 S. Wang, A. Lu and L. N. Zhang, *Prog. Polym. Sci.*, 2016, **53**, 169–206.
11 S. H. Zainal, N. H. Mohd, N. Suhaili, F. H. Anuar, A. M. Lazim and R. Othaman, *J. Mater. Res. Technol.*, 2021, **10**, 935–952.
12 Z. H. Chen, Y. J. Hu, G. Shi, H. Zhuo, M. A. Ali, E. Jamroz, H. L. Zhang, L. X. Zhong and X. W. Peng, *Adv. Funct. Mater.*, 2023, **33**, 2214245.
13 F. D'Acierno, C. A. Michal and M. J. MacLachlan, *Chem. Rev.*, 2023, **123**, 7295–7325.
14 A. Etale, A. J. Onyianta, S. R. Turner and S. J. Eichhorn, *Chem. Rev.*, 2023, **123**, 2016–2048.
15 X. H. Qian, S. Y. Ding, M. R. Nimlos, D. K. Johnson and M. E. Himmel, *Macromolecules*, 2005, **38**, 10580–10589.
16 G. Z. Yang, H. Kong, Y. Chen, B. Liu, D. Z. Zhu, L. Guo and G. Wei, *Carbohydr. Polym.*, 2022, **279**, 118947.
17 X. Z. Li, C. C. Wan, T. Tao, H. Y. Chai, Q. T. Huang, Y. L. Chai and Y. Q. Wu, *Cellulose*, 2024, **31**, 61–99.
18 T. Rosenau, A. Potthast, H. Sixta and P. Kosma, *Prog. Polym. Sci.*, 2001, **26**, 1763–1837.
19 H. B. Zhao, J. H. Kwak, Y. Wang, J. A. Franz, J. M. White and J. E. Holladay, *Carbohydr. Polym.*, 2007, **67**, 97–103.
20 T. Matsumoto, D. Tatsumi, N. Tamai and T. Takaki, *Cellulose*, 2001, **8**, 275–282.
21 L. A. Ramos, D. L. Morgado, O. A. El Seoud, V. C. da Silva and E. Frollini, *Cellulose*, 2011, **18**, 385–392.
22 Y. Wang, Y. L. Zhao and Y. L. Deng, *Carbohydr. Polym.*, 2008, **72**, 178–184.
23 W. Q. Liu, T. Budtova and P. Navard, *Cellulose*, 2011, **18**, 911–920.
24 J. Cai and L. Zhang, *Macromol. Biosci.*, 2005, **5**, 539–548.
25 L. Yan and Z. Gao, *Cellulose*, 2008, **15**, 789–796.
26 G. T. Ciacco, T. F. Liebert, E. Frollini and T. J. Heinze, *Cellulose*, 2003, **10**, 125–132.
27 L. A. Ramos, E. Frollini and T. Heinze, *Carbohydr. Polym.*, 2005, **60**, 259–267.
28 K. Saalwächter, W. Burchard, P. Klüfers, G. Kettenbach, P. Mayer, D. Klemm and S. Dugarmaa, *Macromolecules*, 2000, **33**, 4094–4107.
29 S. Fischer, H. Leipner, K. Thümmler, E. Brendler and J. Peters, *Cellulose*, 2003, **10**, 227–236.
30 S. Sen, J. D. Martin and D. S. Argyropoulos, *ACS Sustainable Chem. Eng.*, 2013, **1**, 858–870.
31 R. P. Swatloski, S. K. Spear, J. D. Holbrey and R. D. Rogers, *J. Am. Chem. Soc.*, 2002, **124**, 4974–4975.
32 J. Wang, Y. Wang, Z. Ma and L. Yan, *Green Energy Environ.*, 2020, **5**, 232–239.
33 Z. Bi, B. Lai, Y. Zhao and L. Yan, *ACS Omega*, 2018, **3**, 2984–2993.
34 M. Egal, T. Budtova and P. Navard, *Cellulose*, 2008, **15**, 361–370.
35 Y. H. Ci, T. Y. Chen, F. Y. Li, X. J. Zou and Y. J. Tang, *Int. J. Biol. Macromol.*, 2023, **252**, 126548.
36 D. J. Tao, F. F. Chen, Z. Q. Tian, K. Huang, S. M. Mahurin, D. E. Jiang and S. Dai, *Angew. Chem., Int. Ed.*, 2017, **56**, 6843–6847.
37 O. Nordness and J. F. Brennecke, *Chem. Rev.*, 2020, **120**, 12873–12902.
38 H. Zhang, J. Wu, J. Zhang and J. S. He, *Macromolecules*, 2005, **38**, 8272–8277.
39 Y. Cao, J. Wu, J. Zhang, H. Q. Li, Y. Zhang and J. S. He, *Chem. Eng. J.*, 2009, **147**, 13–21.
40 A. Xu, L. Chen and J. Wang, *Macromolecules*, 2018, **51**, 4158–4166.
41 X. Zheng, F. Huang, L. H. Chen, L. L. Huang, S. L. Cao and X. J. Ma, *Carbohydr. Polym.*, 2019, **203**, 214–218.
42 K. Fumino, T. Peppel, M. Geppert-Rybczynska, D. H. Zaitsau, J. K. Lehmann, S. P. Verevkin, M. Köckerling and R. Ludwig, *Phys. Chem. Chem. Phys.*, 2011, **13**, 14064–14075.

 This journal is © The Royal Society of Chemistry 2024

Published on 27 2024. Downloaded on 14/05/2026 05:56:35.

43 Y. H. Meng, Z. Q. Pang and C. H. Dong, *Carbohydr. Polym.*, 2017, **163**, 317–323.
44 A. R. Xu, J. J. Wang and H. Y. Wang, *Green Chem.*, 2010, **12**, 268–275.
45 A. R. Xu, L. Chen and J. J. Wang, *Macromolecules*, 2018, **51**, 4158–4166.
46 L. L. Deng, W. Yue, L. H. Zhang, Y. L. Guo, H. B. Xie, Q. Zheng, G. L. Zou and P. Chen, *ACS Sustainable Chem. Eng.*, 2022, **10**, 2158–2168.
47 A. S. Amarasekara, *Chem. Rev.*, 2016, **116**, 6133–6183.
48 D. R. MacFarlane and K. R. Seddon, *Aust. J. Chem.*, 2007, **60**, 3–5.
49 T. L. Greaves, A. Weerawardena, C. Fong, I. Krodkiewska and C. J. Drummond, *J. Phys. Chem. B*, 2006, **110**, 22479–22487.
50 B. Azimi, H. Maleki, V. Gigante, R. Bagherzadeh, A. Mezzetta, M. Milazzo, L. Guazzelli, P. Cinelli, A. Lazzeri and S. Danti, *Cellulose*, 2022, **29**, 3079–3129.
51 B. Meenatchi, V. Renuga and A. Manikandan, *J. Mol. Liq.*, 2017, **238**, 582–588.
52 X. Li, H. C. Li, Z. Ling, D. X. Xu, T. T. You, Y. Y. Wu and F. Xu, *Macromolecules*, 2020, **53**, 3284–3295.
53 X. Y. Wang, W. Q. Zheng, Z. W. Guo, H. Nawaz, T. T. You, X. Li and F. Xu, *Green Chem.*, 2023, **25**, 1597–1610.
54 D. C. M. Ribeiro, R. C. Rebelo, F. De Bon, J. F. J. Coelho and A. C. Serra, *Polymers*, 2021, **13**, 1767.
55 O. Kuzmina, J. Bhardwaj, S. R. Vincent, N. D. Wanasekara, L. M. Kalossaka, J. Griffith, A. Potthast, S. Rahatekar, S. J. Eichhorn and T. Welton, *Green Chem.*, 2017, **19**, 5949–5957.
56 S. Elsayed, M. Hummel, D. Sawada, C. Guizani, M. Rissanen and H. Sixta, *Cellulose*, 2021, **28**, 533–547.
57 X. Y. Wang, T. T. You, W. Q. Zheng, X. Li, S. Chen and F. Xu, *Chem. Eng. J.*, 2024, **483**, 148841.
58 Y. Y. Xie, H. S. Gao, P. Y. Zhang, C. W. Qin, Y. Nie and X. Liu, *ACS Appl. Polym. Mater.*, 2022, **4**, 3598–3607.
59 Y. Fukaya, K. Hayashi, M. Wada and H. Ohno, *Green Chem.*, 2008, **10**, 44–46.
60 W. Yue, L. H. Zhang, L. L. Deng, Y. L. Guo, Q. Q. Xu, W. Peng, P. Chen, H. B. Xie, G. L. Zou and S. M. Liang, *Green Chem.*, 2021, **23**, 9669–9682.
61 A. Shakeel, H. Mahmood, U. Farooq, Z. Ullah, S. Yasin, T. Iqbal, C. Chassagne and M. Moniruzzaman, *ACS Sustainable Chem. Eng.*, 2019, **7**, 13586–13626.
62 Y. X. Lv, J. Wu, J. M. Zhang, Y. H. Niu, C. Y. Liu, J. S. He and J. Zhang, *Polymer*, 2012, **53**, 2524–2531.
63 Y. Xu, H. L. Shao, Y. P. Zhang and X. C. Hu, *J. Mater. Sci.*, 2005, **40**, 5355–5358.
64 F. Lu, J. Song, B. W. Cheng, X. J. Ji and L. J. Wang, *Cellulose*, 2013, **20**, 1343–1352.
65 W. Q. Li, Z. M. Wang, M. F. Li and N. Normakhamatov, *Cellulose*, 2021, **28**, 2849–2861.
66 X. R. Zhang, Q. J. Fu, Y. C. Wang, H. A. Zhao, S. W. Hao, C. Ma, F. Xu and J. Yang, *Adv. Funct. Mater.*, 2023, 2307400, DOI: **10.1002/adfm.202307400**.
67 T. Kondo, *Cellulose*, 1997, **4**, 281–292.
68 S. S. Rumi, S. Liyanage and N. Abidi, *Cellulose*, 2021, **28**, 2021–2038.
69 B. Q. Wang, Y. Nie, Z. Q. Kang and X. Liu, *Int. J. Biol. Macromol.*, 2023, **225**, 1374–1383.
70 C. Y. Chen, M. J. Chen, X. Q. Zhang, C. F. Liu and R. C. Sun, *J. Agric. Food Chem.*, 2014, **62**, 3446–3452.
71 Y. C. Peng, D. J. Gardner, Y. Han, A. Kiziltas, Z. Y. Cai and M. A. Tshabalala, *Cellulose*, 2013, **20**, 2379–2392.
72 J. M. Zhao, W. J. Ge, J. B. Shuai, X. L. Gao, F. S. Zhang and X. H. Wang, *Macromol. Rapid Commun.*, 2023, **44**, 2300175.
73 L. Cammarata, S. G. Kazarian, P. A. Salter and T. Welton, *Phys. Chem. Chem. Phys.*, 2001, **3**, 5192–5200.
74 Z. S. Fan, J. B. Chen, W. J. Guo, F. Ma, S. Q. Sun and Q. Zhou, *RSC Adv.*, 2017, **7**, 41004–41010.
75 Y. Q. Deng, H. F. Wang, K. F. Zhang, J. Qiu and L. F. Yan, *Adv. Sustainable Syst.*, 2022, **6**, 2100191.
76 K. Chen, J. Huang, J. Yuan, S. Qin, P. Huang, C. Wan, Y. You, Y. Guo, Q. Xu and H. Xie, *Energy Storage Mater.*, 2023, **63**, 102963.
77 D. P. Dubal, O. Ayyad, V. Ruiz and P. Gómez-Romero, *Chem. Soc. Rev.*, 2015, **44**, 1777–1790.
78 J. Yin, W. L. Zhang, N. A. Alhebshi, N. Salah and H. N. Alshareef, *Adv. Energy Mater.*, 2021, **11**, 2100201.
79 A. T. Zhu, J. Huang, H. B. Xie, W. Yue, S. D. Qin, F. Z. Zhang and Q. Q. Xu, *Chem. Eng. J.*, 2022, **446**, 137032.
80 Y. Cheng, X. Y. Ren, L. J. Duan and G. H. Gao, *J. Mater. Chem. C*, 2020, **8**, 8234–8242.
81 K. F. Zhang, Y. J. Pang, C. Z. Chen, M. Wu, Y. X. Liu, S. T. Yu, L. Li, Z. Ji and J. H. Pang, *Carbohydr. Polym.*, 2022, **293**, 119673.
82 X. F. Zhang, J. Q. Zhao, T. Xia, Q. Y. Li, C. H. Ao, Q. H. Wang, W. Zhang, C. H. Lu and Y. L. Deng, *Energy Storage Mater.*, 2020, **31**, 135–145.
83 P. X. Zhang, M. Li, Y. D. Jing, X. M. Zhang, S. P. Su, J. Zhu and N. Y. Yu, *J. Mater. Sci.*, 2023, **58**, 1694–1707.
84 Z. Y. Peng, Y. B. Zou, S. Q. Xu, W. B. Zhong and W. T. Yang, *ACS Appl. Mater. Interfaces*, 2018, **10**, 22190–22200.
85 Y. Q. Deng, H. F. Wang, K. F. Zhang, J. W. Shao, J. Qiu, J. Wu, Y. H. Wu and L. F. Yan, *Nanoscale*, 2021, **13**, 3010–3018.